Coexistence of Midgap Antiferromagnetic and Mott States in Undoped, Hole- and Electron-Doped Ambipolar Cuprates

Xinmao Yin,[1,2,3,9] Shengwei Zeng,[2,3] Tanmoy Das,[3,5,8] G. Baskaran,[6,7] Teguh Citra Asmara,[1,2,3] Iman Santoso,[1,2] Xiaojiang Yu,[1] Caozheng Diao,[1] Ping Yang,[1] Mark B. H. Breese,[1,3] T. Venkatesan,[2,4] Hsin Lin,[3,5,*] Ariando,[2,3,†] and Andrivo Rusydi[1,2,3,‡]

[1]*Singapore Synchrotron Light Source, National University of Singapore, 5 Research Link, Singapore 117603, Singapore*
[2]*NUSSNI-NanoCore, National University of Singapore, Singapore 117576, Singapore*
[3]*Department of Physics, National University of Singapore, Singapore 117542, Singapore*
[4]*Department of Electrical and Computer Engineering, National University of Singapore, Singapore 117583, Singapore*
[5]*Centre for Advanced 2D Materials and Graphene Research Centre, National University of Singapore, Singapore 117546, Singapore*
[6]*The Institute of Mathematical Sciences, Chennai 600041, India*
[7]*Perimeter Institute for Theoretical Physics, Waterloo, Ontario N2L 2Y5, Canada*
[8]*Department of Physics, Indian Institute of Science, Bangalore 560012, India*
[9]*SZU-NUS Collaborative Innovation Center for Optoelectronic Science & Technology, Key Laboratory of Optoelectronic Devices and Systems of Ministry of Education and Guangdong Province, College of Optoelectronic Engineering, Shenzhen University, Shenzhen 518060, China*

(Received 7 September 2015; published 12 May 2016)

We report the first observation of the coexistence of a distinct midgap state and a Mott state in undoped and their evolution in electron and hole-doped ambipolar $Y_{0.38}La_{0.62}(Ba_{0.82}La_{0.18})_2Cu_3O_y$ films using spectroscopic ellipsometry and x-ray absorption spectroscopies at the O K and Cu $L_{3,2}$ edges. Supported by theoretical calculations, the midgap state is shown to originate from antiferromagnetic correlation. Surprisingly, while the magnetic state collapses and its correlation strength weakens with dopings, the Mott state in contrast moves toward a higher energy and its correlation strength increases. Our result provides important clues to the mechanism of electronic correlation strengths and superconductivity in cuprates.

DOI: 10.1103/PhysRevLett.116.197002

Soon after the discovery of high-temperature superconductivity in copper-oxide base alloys [1], two parallel theoretical concepts were proposed for the mechanism of unconventional superconductivity, namely, a resonant valence bond theory [2–4] in the strong-correlation regime and a spin fluctuation theory [5–7] in the weak-correlation regime. These two theoretical paradigms were primarily influenced by the nature of the insulating state in the parent compound. The resonant valence bond theory is based on the assumption that the cuprates at half-filling are Mott insulators in which double occupancy in each Cu site is prohibited by strong Coulomb interaction, and the antiferromagnetic (AFM) order that occurs below Néel temperature is a consequence rather than a cause of the Mott-insulating phase. On the other hand, the spin fluctuation theory proposed that the AFM phase is driven by Fermi surface instability induced symmetry breaking and a strong AFM interaction at half-filling leads to insulating behavior.

Even though experiments have shown evidence of each scenario independently, e.g., Mott gap features from optical conductivity [8,9] and x-ray absorption spectroscopy (XAS) [10] measurements for the former and various competing orders [11,12], Hall-effect and quantum oscillation measurements [13,14], for the latter, a direct, systematic experiment that can measure and simultaneously link the strong and weak coupling scales is still lacking. Another important unresolved problem is the origin of the asymmetry between hole- and electron-doped cuprates in which most studies were done on different parent compounds, which had different crystallography and electronic band structures. It is now possible to study the evolution of electronic structure from hole- to electron-doped cuprates within the same parent compound in an ambipolar cuprate of $Y_{1-z}La_z(Ba_{1-x}La_x)_2Cu_3O_y$ [15,16]. Therefore, such an experiment is then crucial for understanding the origin of normal, insulating state and evolution of electronic correlation strengths as a function of both hole- and electron doping in cuprates, particularly in the low-carrier-concentration regime.

Here, we design an experiment to reveal comprehensively the evolution of electronic structure of unique ambipolar cuprates $Y_{1-z}La_z(Ba_{1-x}La_x)_2Cu_3O_y$ (YLBLCO), in undoped, hole- and electron-doped cases, using a combination of high-resolution spectroscopic ellipsometry (SE) and XAS at the O K and Cu $L_{3,2}$ edges. Our detailed analysis is further supported by a self-consistent momentum-resolved density-wave fluctuation (MRDF) theory for calculating the self-energy correction by including the antiferromagnetic order and spin and charge density fluctuations.

High-quality $Y_{0.38}La_{0.62}(Ba_{0.82}La_{0.18})_2Cu_3O_y$ (about 260 nm) films are grown on (001) $LaAlO_3$ using pulsed

laser deposition [15]. Since the oxygen content cannot be measured precisely for hole (p-type) and electron (n-type) films, in our discussion we refer to the carrier concentrations, which are obtained from Hall-effect measurements at room temperature (~300 K). Eleven high-quality single crystalline films are specially prepared to represent for the insulating case ($P0$), p-type ($P1$–$P5$) and n-type ($N1$–$N5$). The carrier concentrations of the p-type samples are $P1 = 9.7 \times 10^{16}\,\mathrm{cm}^{-3}$, $P2 = 2.2 \times 10^{20}\,\mathrm{cm}^{-3}$, $P3 = 7.9 \times 10^{20}\,\mathrm{cm}^{-3}$, $P4 = 1.3 \times 10^{21}\ \mathrm{cm}^{-3}$, and $P5 = 2.5 \times 10^{21}\ \mathrm{cm}^{-3}$. The $P0$ is an insulating sample, with carrier concentration beyond the limit of the transport measurement. The carrier concentrations of n-type samples are $N1 = 6.3 \times 10^{16}\ \mathrm{cm}^{-3}$, $N2 = 3.6 \times 10^{20}\ \mathrm{cm}^{-3}$, $N3 = 4.7 \times 10^{20}\ \mathrm{cm}^{-3}$, $N4 = 7 \times 10^{20}\ \mathrm{cm}^{-3}$, and $N5 = 2.3 \times 10^{21}\ \mathrm{cm}^{-3}$. We note that all samples are in the low-doping regime and samples of $P4$ ($T_c \sim 8$ K) and $P5$ ($T_c \sim 34$ K) are superconductors below T_c [16]. The magnetization and transport data also support high-quality samples [17]. High-resolution x-ray diffraction measurements show that our films are untwinned and the crystallographic structure of the films reveals a perfect coherent interface between the film and substrate (see Supplemental Material, Fig. S1 [17]). The crystal structure and proposed phase diagram of YLBLCO based on transport measurements are shown in Figs. 1(a)–1(b), respectively. The optical conductivity is determined using spectroscpic ellipsometry (SE). The XAS at the O K edge ($1s \rightarrow 2p$) and Cu $L_{2,3}$ edges ($2p \rightarrow 3d$) are obtained using linearly polarized XAS from the surface, interface, and nanostructure science (SINS) beam line at the Singapore Synchrotron Light Source, via a total electron yield mode. All the experiments are done at room temperature. The details of samples and experimental methods are explained in the Supplemental Material [17].

A new and important observation is a distinct, midinfrared peak (labeled a) at 0.9 eV in the optical conductivity obtained from SE measurements [see Figs. 1(c)–1(d)] for $P0$ (undoped). At higher energy, a peak (labeled b) near 1.6 eV is observed and ascribed to the charge-transfer transitions (Mott gap) [32], similar to other cuprates [8,33]. Intriguingly, peak a is very narrow, with half width at half maximum of 0.06 eV, three times sharper than that of peak b (~0.17 eV). Meanwhile, the maximum intensity of peak a is ~500 $\Omega^{-1}\,\mathrm{cm}^{-1}$, which is surprisingly comparable to that of peak b (~700 $\Omega^{-1}\,\mathrm{cm}^{-1}$). Supported with MRDF calculations (as discussed below), we argue that peak a is ascribed to the antiferromagnetic gap, while peak b is related to the charge-transfer transition from the magnetic bands to the Mott-Hubbard bands [18]. We note that a similar midgap state (at ~1 eV) was also observed in other cuprates; however, the origin was not understood [33]. Interestingly, in spectra of both p-type and n-type samples, peak a gets broader and spectral weight of both peaks a and b enhances. As carrier concentrations increase, peak a shifts to lower energy and at the same time a Drude response emerges, while peak b shifts toward higher energy

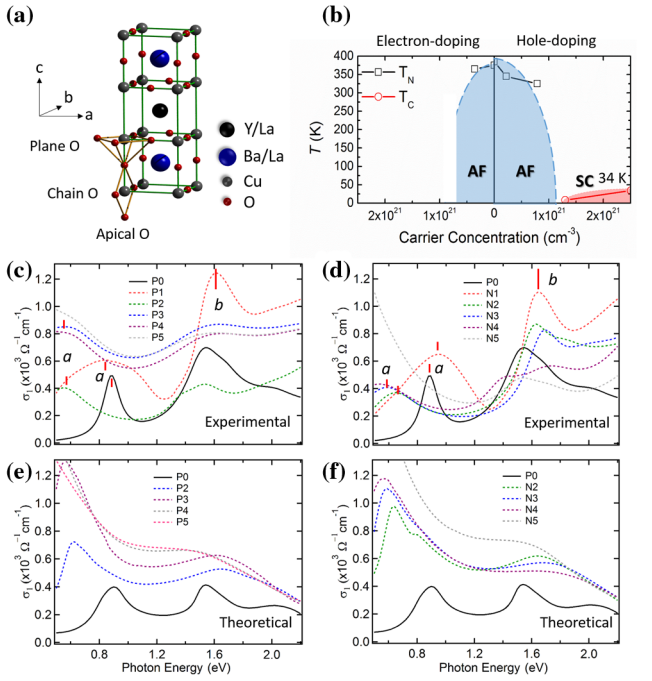

FIG. 1. (a) Crystal structure and (b) phase diagram of p-type and n-type YLBLCO. Note that while T_c is from our transport measurements, T_N is estimated according to the relationship between the Nèel temperature and carrier concentration from Ref. [16]. Optical conductivity (σ_1) of (c) p-type and (d) n-type YLBLCO for various carrier concentrations and insulator $P0$ from spectroscopic ellipsometry measurements. Theoretical calculations of σ_1 of (e) p-type and (f) n-type YLBLCO for various carrier concentrations and insulator $P0$.

and gets broader. Particularly for the n type, the shift and broadening of peak b are rather significant. The evolution of peak a, peak b, and overall shape of optical conductivity is clearly different for the p- and n-type, suggesting that holes and electrons behave differently in modifying the electronic structure of cuprates. The presence of the new peak a and the different behavior between p- and n-type are further revealed with XAS as discussed below.

Figure 2 shows XAS at O K (low-energy region) and Cu L_3 edges for in-plane polarization ($\mathbf{E} \perp c$). Let us discuss XAS at the O K edge first. This transition is particularly sensitive to O $2p$ – Cu $3d$ hybridization; thus, it probes unoccupied Cu $3d$ orbitals. Interestingly, for $P0$ two prepeaks are observed: a new peak at ~528.3 eV (labeled A), and a peak at ~528.9 eV (labeled B). The energy separation between peaks A and B [Fig. 2(a)] from XAS is the same as the energy difference between peaks a and b from SE [Fig. 1(c)]. The consistency of energy different between the two experiments strongly supports the observation of new midgap states (peak A and peak a). Peak B is known as the transition into the upper Hubbard band (UHB) [34,35]. Supported by our MRDF calculations and SE data, peak A is related with the upper (unoccupied) magnetic band (UMB).

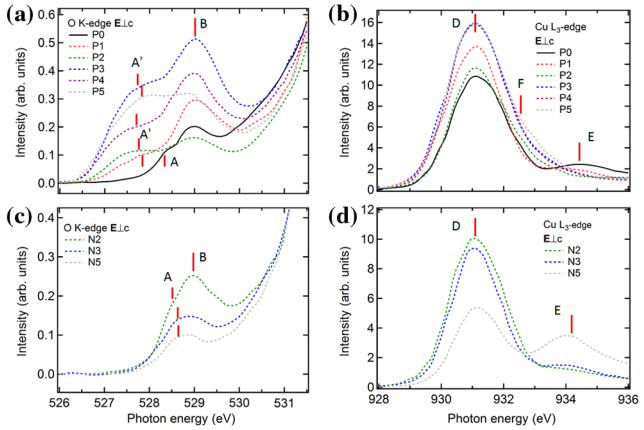

FIG. 2. Low-energy region (preedge peak) of the O K-edge absorption spectra of (a) p-type and (c) n-type YLBLCO with various carrier concentrations including an insulator $P0$ for $\mathbf{E}\perp c$. Cu L_3 edge absorption spectra of (b) p-type and (d) n-type YLBLCO with various carrier concentration including an insulator $P0$ for $\mathbf{E}\perp c$.

The behavior of peak A and peak B differs between p- and n-type samples. For p-type YLBLCO, as the carrier concentration increases, a hole-doped peak related to doped holes occurs, while the peak A shifts towards lower energy and emerges with the hole-doped peak [peak $A\prime$, Fig. 2(a)]. Supported by our SE and theoretical calculations, for the p-type sample the first prepeak at the O K edge (peak A') is a mixing of the hole-doped peak [or Zhang-Rice (ZR) feature] and UMB peak. Note that the UMB peak has never been discussed in any previous XAS studies of hole-doped $YBa_2Cu_3O_{7-\delta}$ [36–38]. By combining high-resolution XAS and SE measurements on the very same sample and simultaneously analyzing those experimental data as well as supporting theoretical calculations, one can now distinguish UMB from the others. The UHB peak (or peak B) stays almost at the same energy but its intensity varies as a function of carrier concentration [cf. Fig. 2(a)]. We observe an unusual behavior of peak B in the p-type YLBLCO. The unusual behavior of a spectral weight transfer of those peaks involving such a broad energy range shows the importance of strong electronic correlations and the complexity of the systems [39]. In other cuprates, the intensity of peak B decreases upon hole doping due to strong electronic correlations yielding to spectral weight transfer [10,40]. However, the intensity of peak B for $P3$ is higher than that for $P2$ [Fig. 2(a)]. These unusual increases can be explained by Cu L_3 edge XAS results, as discussed later.

For n-type YLBLCO, peak A decreases in intensity and shifts toward higher energy as the carrier concentration increases [Fig. 2(c)]. As shown in previous study that the ZR feature occurred as occupied states in n-type cuprates [41], the presence of peak A in n-type YLBLCO is strong evidence that peak A is not the ZR feature. On the other hand, the intensity of peak B also reduces but its energy position is retained.

For sample $P0$, the XAS at the Cu L_3 edge consists of a white line feature (labeled D) at ~931.1 eV and a satellite band (labeled E) at ~934.3 eV [Fig. 2(b)]. For p-type YLBLCO, as the carrier concentration increases, peak D increases in intensity accompanied by the appearance of a shoulder (labeled F) just above the white line feature, while peak E decreases. We note that peak D saturates at a certain carrier concentration ($P3$). The intensity of peak F increases as the carrier concentration increases. According to previous XAS studies on other cuprates [34,38,41–43], the white line feature D is related to Cu-$2p \rightarrow 3d$ transitions, which involve Cu^{2+} ions and peak E is ascribed to the hybridization of Cu-$4s$ (Cu^{1+}) with Cu-$3d$ states, while peak F has been ascribed to ligand hole states [34,42]. As the carrier concentration increases, the increase of peak D and the decrease of peak E suggest that doping holes in YLBLCO change the valence of Cu from Cu^{1+} to Cu^{2+} in the CuO_2 plane (CuO_3 chains) [17]. This is consistent with the increase of the UHB feature in the O K edge XAS spectra as discussed above [44]. Furthermore, the presence of Cu^{1+} in the CuO_2 plane may be due to the substitution of La^{3+} for Ba^{2+} and the oxygen defect or intercalation.

For n-type YLBLCO [Fig. 2(d)], the intensity of the white line feature D decreases as the carrier concentration increases, while the intensity of peak E increases. The result suggests that part of the electrons go into the Cu atom, which changes from Cu^{2+} to Cu^{1+} ions. This is consistent with the observation that peak B decreases as the carrier concentration increases in Fig. 2(c).

To explain these unprecedented data, we perform a full momentum dependent self-energy formalism for a single CuO_2 band within the Hubbard model by treating the Coulomb interaction as being doping dependent [17,45]. The theoretical results are shown in Fig. 3. The optical and XAS data shown above collectively indicate that an antiferromagnetic order occurs in the itinerant states, creating an insulating gap, while the localized states are already separated to higher energy before the magnetic ordering sets in. The dominant interaction that creates such an itinerant and localization duality is predominantly made of density fluctuations in the spin and charge sectors. The calculations show the dominance of dynamical correlation in the presence of a van Hove singularity at $k = (\pi, 0)$. Such fluctuation dispersions have been observed by resonant-inelastic x-ray scattering in $La_{2-x}Sr_xCuO_4$, from the undoped to the heavily overdoped regime [46,47].

Our computed self-energy dressed spectral weight spectrum is presented in Fig. 3(a) for three representative dopings. Four subbands are clearly visible at all dopings, in which the two low-energy bands are split by magnetic ordering, while each magnetic band is further split by the anomalous energy dependence of the self-energies, shown in Figs. 3(b) and 3(c). The strength of the correlation is dominant in the momentum regions, and gradually decreases as we move towards the nodal direction as

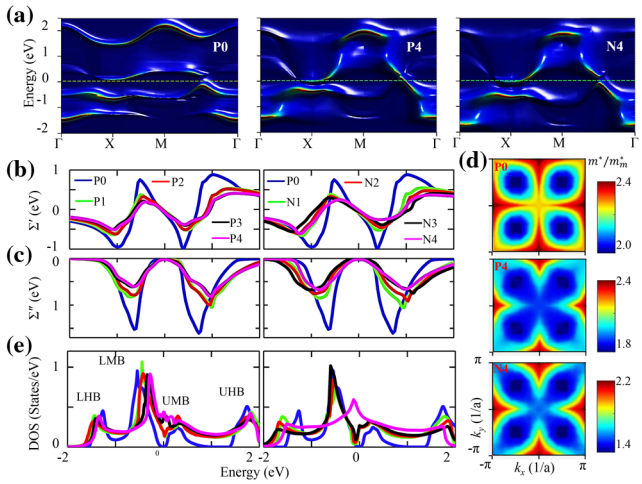

FIG. 3. (a) The computed self-energy dressed spectral weight spectrum for three representative dopings, insulating $P0$, $P4$, and $N4$. (b) Real (Σ') and (c) imaginary part (Σ'') of self-energy of p-type (left) and n-type (right) YLBLCO for various carrier concentrations and $P0$. (d) The computed k-dependent mass renormalization factor for three representative dopings, $P0$, $P4$, and $N4$. (e) DOS of p-type (left) and n-type (right) YLBLCO for various carrier concentrations and $P0$.

manifested in the computed k-dependent mass renormalization factor shown in Fig. 3(d).

The doping dependence of the self-energy reveals a surprising trend. With both increasing hole and electron doping, the correlation strength weakens, causing the self-energy to reduce in amplitude. Since the overall shape of the self-energy remains the same, as it becomes flatter with doping (i.e., the renormalization effect decreases), the energy scale where real-part changes slope and the imaginary part acquires peak gradually shifts to higher energy. As a result the self-energy generated localized Mott-like bands shift to higher energy as the self-energy weakens. This is a characteristically opposite behavior to what is expected within typical Mott physics where a weaker correlation strength means a smaller Mott gap. In the former case, however, the spectral weight of the high-energy band loses intensity and the corresponding spectral weight is gradually shifted to the itinerant strength. This behavior of the self-energy is manifested in the doping dependence of the four peaks in the DOS, shown in Fig. 3(e).

We next compute optical conductivity quantity using the Kubo formula of linear response theory. It is shown in Figs. 1(e) and 1(f), and is in good qualitative agreement with the experimental results. The optical conductivity at half-filling exhibits three peaks: the lowest energy peak [e.g., ~0.9 eV for $P0$ as shown in Fig. 1(c)] reflects the magnetic gap; the intermediate energy peak (e.g., ~1.6 eV) stems from the optical transition across the magnetic bands to the Mott-like bands; the higher energy peak (e.g., ~2.0 eV) arises from the transition across the two Mott-like bands. Note that the magnetic gap in the optical spectrum is relatively sharper in both theory and experimental data, yet it has been missed by earlier studies.

We extract the energy position of the major peaks in Figs. 1 and 2, which are shown in Figs. 4(a) and 4(b), and compare them with our theoretical results for p-type and n-type YLBLCO (see also Supplemental Material, Table S1 [17]). The experiments and theory are in good accord. In the low carrier-concentration regimes (for both p-type and n-type YLBLCO), the magnetic gap exhibits a rapid decrease, while the charge-transfer gap provides an opposite carrier-concentration dependence to the magnetic gap. For higher carrier-concentration regimes, the magnetic gap is shifted down below 0.5 eV (measurement limit) and the charge-transfer gap exhibits a decrease.

By combining the XAS and optical conductivity and supported by theoretical calculations, we propose a pictorial model of electronic structures of the YLBLCO as a function of doping as shown in Fig. 4(c). The unoccupied bands are related to the corresponding peaks in the XAS spectra as discussed above, while the energy differences of each band are obtained from the optical gap in optical conductivity spectra and the energy difference of peaks in the XAS spectra (see also Supplemental Material for theoretical calculations XAS [17]).

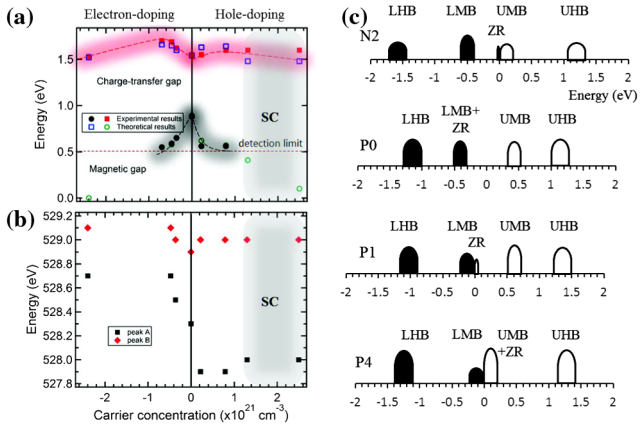

FIG. 4. (a) Contrasting carrier-concentration dependences of the magnetic and charge-transfer gaps in p-type and n-type YLBLCO. Present theoretical and experimental results (measured by spectroscopic ellipsometry). (b) Carrier-concentration dependences of the energy position of peaks A (A'), and B for p-type and n-type YLBLCO extracted XAS at the O K edge (cf. Fig. 2). The shadow and the dashed lines are to guide the eye. (c) Proposed electronic structure model of samples $N2$, $P0$, $P1$, and $P4$, as derived from the analyses of XAS and SE data. The black (empty) bands are occupied (unoccupied) by electrons. There are lower (LHB) and upper Hubbard bands (UHB) separated by the Mott-Hubbard gap, lower (LMB) and upper magnetic bands (UMB) separated by the antiferromagnetic gap, and the Zhang-Rice (ZR) feature. The "0 eV" represent the Fermi level. We note that for $P0$ and n-type cases the ZR feature occurs below the Fermi level and is accessible in SE but not in XAS. While for p-type cases, the ZR feature occurs above the Fermi level and is accessible in both SE and XAS.

Cuprates exhibit various low-energy gaps with different doping and temperature dependencies such as the AFM gap, pseudogap, charge-density-wave (CDW) gap, and others. The presently observed midinfrared (MIR) gap cannot arise from the CDW, since CDW arises at finite doping, and often exhibits a dome like structure centering around 12.5% doping [48]. On the other hand, the doping dependence of the MIR we observe here decreases monotonically from half-filling which resembles the doping dependence of either an AFM gap or the pseudogap behavior. In hole-doped cuprates, the AFM gap disappears rapidly with doping, while pseudogap behavior persists to higher doping. Our measured small quasiparticle gap at finite doping matches well with the AFM gap measured by other techniques [10,33,34], while the pseudogap value deviates from our observations in these extremely underdoped samples [49,50]. Furthermore, we observe asymmetry in the quasiparticle magnetic gap within the same sample. The asymmetry has also been seen in the spin excitation spectrum on other electron and hole-doped cuprates [51]. Therefore, we conclude that the MIR gap we observe here is due to the AFM ordering.

In summary, using the combination of SE, XAS at O K and Cu $L_{3,2}$ edges and supported by self-consistent momentum-resolved density-wave fluctuation calculations, the coexistence of midgap antiferromagnetic and Mott states in undoped, hole- and electron-doped ambipolar $Y_{0.38}La_{0.62}(Ba_{0.82}La_{0.18})_2Cu_3O_y$ films is observed. As a function of dopings, the magnetic state collapses and its correlation strength weakens. In contrast the Mott state moves toward a higher energy and its correlation strength increases. Our result unifies a long-standing puzzle about the correlation strengths and resolves the origin of asymmetry between electron doping and hole doping in cuprates. Furthermore, the methodology presented here can be applied to study electronic correlations and the electronic structure of correlated electron systems in general.

We acknowledge George Sawatzky, R. S. Markiewicz, and Daniel Khomskii for their discussions and valuable comments. This work is supported by the Singapore National Research Foundation under its Competitive Research Funding (No. NRF-CRP 8-2011-06 and No. NRF2008NRF-CRP002024) and its NRF fellowship (NRF Award No. NRF-NRFF2013-03), MOE-AcRF Tier-2 (MOE2015-T2-1-099, and MOE2010-T2-2-121), NUS-YIA, FRC (R-144-000-368-112, R-144-000-346-112 and R-144-000-364-112), and NUS Core Support C-380-003-003-001.

X. Y., S. Z., and T. D. contributed equally to this work.

*nilnish@gmail.com
†ariando@nus.edu.sg
‡phyandri@nus.edu.sg

[1] J. G. Bednorz and K. A. Müller, Z. Phys. B **64**, 189 (1986).
[2] P. W. Anderson, Science **235**, 1196 (1987).
[3] S. A. Kivelson, D. S. Rokhsar, and J. P. Sethna, Phys. Rev. B **35**, 8865(R) (1987).
[4] G. Baskaran, Z. Zou, and P. W. Anderson, Solid State Commun. **63**, 973 (1987).
[5] V. J. Emery, Phys. Rev. Lett. **58**, 2794 (1987).
[6] P. Monthoux, A. V. Balatsky, and D. Pines, Phys. Rev. Lett. **67**, 3448 (1991).
[7] D. J. Scalapino, Rev. Mod. Phys. **84**, 1383 (2012).
[8] S. Uchida, T. Ido, H. Takagi, T. Arima, Y. Tokura, and S. Tajima, Phys. Rev. B **43**, 7942 (1991).
[9] D. N. Basov and T. Timusk, Rev. Mod. Phys. **77**, 721 (2005).
[10] C. T. Chen *et al.*, Phys. Rev. Lett. **66**, 104 (1991).
[11] S. A. Kivelson, I. P. Bindloss, E. Fradkin, V. Oganesyan, J. M. Tranquada, A. Kapitulnik, and C. Howald, Rev. Mod. Phys. **75**, 1201 (2003).
[12] E. Fradkin, S. A. Kivelson, and J. M. Tranquada, Rev. Mod. Phys. **87**, 457 (2015).
[13] N. Doiron-Leyraud, C. Proust, D. LeBoeuf, J. Levallois, J.-B. Bonnemaison, R. Liang, D. A. Bonn, W. N. Hardy, and L. Taillefer, Nature (London) **447**, 565 (2007).
[14] N. Barisic *et al.*, Nat. Phys. **9**, 761 (2013).
[15] S. W. Zeng *et al.*, Phys. Rev. B **86**, 045124 (2012).
[16] K. Segawa, M. Kofu, S-H. Lee, I. Tsukada, H. Hiraka, M. Fujita, S. Chang, K. Yamada, and Y. Ando, Nat. Phys. **6**, 579 (2010).
[17] See Supplemental Material at http://link.aps.org/supplemental/10.1103/PhysRevLett.116.197002, which includes Refs. [18-31], for the detail of samples, the methods using in this Letter and the corresponding figures and table, including High-resolution x-ray Diffraction measurements, x-ray Absorption Spectroscopy measurements, Spectroscopic Ellipsometry measurements, and theoretical calculations of optical conductivity and x-ray absorption spectroscopy.
[18] R. J. Cava, A. W. Hewat, E. A. Hewat, B. Batlogg, M. Marezio, K. M. Rabe, J. J. Krajewski, W. F. Peck, Jr., and L. W. Rupp, Jr., Physica (Amsterdam) **165C**, 419 (1990).
[19] J. D. Jorgensen, B. W. Veal, A. P. Paulikas, L. J. Nowicki, G. W. Crabtree, H. Claus, and W. K. Kwok, Phys. Rev. B **41**, 1863 (1990).
[20] D. C. Peets *et al.*, Phys. Rev. Lett. **103**, 087402 (2009).
[21] R. M. A. Azzam and N. M. Bashara, *Ellipsometry and Polarized Light* (North-Holland Pub. Co., Amsterdam, 1977).
[22] H. Fujiwara, *Spectroscopic Ellipsometry: Principles and Applications* (John Wiley & Sons, Chichester, 2007).
[23] T. C. Asmara *et al.*, Nat. Commun. **5**, 3663 (2014).
[24] I. Santoso, R. S. Singh, P. K. Gogoi, T. C. Asmara, D. Wei, W. Chen, A. T. S. Wee, V. M. Pereira, and A. Rusydi, Phys. Rev. B **89**, 075134 (2014).
[25] R. Rauer, G. Neuber, J. Kunze, J. Bäckström, and M. Rübhausen, Rev. Sci. Instrum. **76**, 023910 (2005).
[26] X. Yin *et al.*, NPG Asia Mater. **7**, e196 (2015).
[27] M. Born, E. Wolf, and A. B. Bhatia, *Principles of Optics: Electromagnetic Theory of Propagation, Interference and*

Diffraction of Light (Cambridge University Press, Cambridge, 2000).
[28] B. Harbecke, Appl. Phys. B **39**, 165 (1986).
[29] A. B. Kuzmenko, Rev. Sci. Instrum. **76**, 083108 (2005).
[30] T. Ahmed, T. Das, J. J. Kas, H. Lin, B. Barbiellini, F. D. Vila, R. S. Markiewicz, A. Bansil, and J. J. Rehr, Phys. Rev. B **83**, 115117 (2011).
[31] R. S. Markiewicz, T. Das, and A. Bansil, Phys. Rev. B **82**, 224501 (2010).
[32] J. Zaanen, G. A. Sawatzky, and J. W. Allen, Phys. Rev. Lett. **55**, 418 (1985).
[33] Y. Onose, Y. Taguchi, K. Ishizaka, and Y. Tokura, Phys. Rev. B **69**, 024504 (2004).
[34] N. Nücker, E. Pellegrin, P. Schweiss, J. Fink, S. L. Molodtsov, C. T. Simmons, G. Kaindl, W. Frentrup, A. Erb, and G. Müller-Vogt, Phys. Rev. B **51**, 8529 (1995).
[35] M. Taguchi *et al.*, Phys. Rev. Lett. **95**, 177002 (2005).
[36] M. Merz *et al.*, Phys. Rev. Lett. **80**, 5192 (1998).
[37] A. Krol *et al.*, Phys. Rev. B **45**, 2581 (1992).
[38] D. G. Hawthorn *et al.*, Phys. Rev. B **84**, 075125 (2011).
[39] M. B. J. Meinders, H. Eskes, and G. A. Sawatzky, Phys. Rev. B **48**, 3916 (1993).
[40] E. Pellegrin *et al.*, Phys. Rev. B **47**, 3354 (1993).
[41] M. Alexander *et al.*, Phys. Rev. B **43**, 333 (1991).
[42] C. T. Chen, L. H. Tjeng, J. Kwo, H. L. Kao, P. Rudolf, F. Sette, and R. M. Fleming, Phys. Rev. Lett. **68**, 2543 (1992).
[43] C. F. J. Flipse, G. van der Laan, A. L. Johnson, and K. Kadowaki, Phys. Rev. B **42**, 1997 (1990).
[44] The peak F is obscure in the $\mathbf{E}\perp c$ spectra (Supplemental Material, Fig. S3 [17]), since it mixes with the high intensity white line. The intensity of peak E of $\mathbf{E}\perp c$ spectrum is much higher than that of $\mathbf{E}\sim\|c$ spectrum for insulating $P0$ (Supplemental Material, Fig. S3 [17]).
[45] T. Das, R. S. Markiewicz, and A. Bansil, Adv. Phys. **63**, 151 (2014).
[46] M. Le Tacon *et al.*, Nat. Phys. **7**, 725 (2011).
[47] M. P. M. Dean *et al.*, Nat. Mater. **12**, 1019 (2013).
[48] G. Ghiringhelli *et al.*, Science **337**, 821 (2012).
[49] S. Hüfner, M. A. Hossain, A. Damascelli, and G. A. Sawatzky, Rep. Prog. Phys. **71**, 062501 (2008).
[50] M. Hashimoto, I. M. Vishik, R.-H. He, T. P. Devereaux, and Z.-X. Shen, Nat. Phys. **10**, 483 (2014).
[51] W. S. Lee *et al.*, Nat. Phys. **10**, 883 (2014).